nature communications

Article

https://doi.org/10.1038/s41467-025-57064-6

Histamine-modulated wettability switching in G-protein-coupled receptor inspired nanochannel for potential drug screening and biosensing

Received: 20 March 2024

Accepted: 11 February 2025

Published online: 20 February 2025

Check for updates

Qi Zhao[1,2,3], Xu-Qin Ran[3], Zhu-Ying Yan[4], Hai-Long Qian[3] & Xiu-Ping Yan[1,2,3,4,5]

Histamine receptor, one typical G-protein-coupled receptor (GPCR), can be activated by histamine and form the most important drug targets involved in allergy and reflux diseases. Here, we report an artificial model to mimic the wettability-induced activation of natural GPCRs via histamine-modulated enhancement of wettability in a bionic nanochannel. The artificial receptor is constructed by introducing key recognition factors in nature, L-lysine modified fluorescein isothiocyanate (L-lysine-FITC), into a conical nanochannel. The conductance of the L-lysine-FITC-modified nanochannel increases with the histamine-induced wettability enhancement due to the various interactions between histamine and L-lysine-FITC molecules including hydrogen bonding and π-π interactions, as well as the proton transfer reaction. This study represents a crucial step towards the design of artificial GPCRs with wettability-induced activation and provides an opportunity to construct artificial models of GPCRs in a non-lipid environment. The developed artificial receptor has great potential application in medicinal chemistry, biosensors, and healthcare systems.

Cellular signal transduction plays a crucial role in maintaining and regulating the balance of intracellular and extracellular environments, which largely depends on the controlled transport of messenger molecules across the membrane proteins[1]. G-protein-coupled receptors (GPCRs) as the largest class of membrane proteins in the human genome mediate many important physiological processes, making them attractive drug targets[2–4]. It is worth noting that extracellular signals are transferred to the intracellular sides of cells by activating GPCRs. Briefly, the activation of GPCRs is induced by the wettability changes of the hydrophobic layer inside the receptor when ligand-binding events occur in living organisms[5,6]. Histamine (Hm) receptor, one typical GPCR, is an important mediator of signalling that is responsible to regulate human autoimmunity[7–10]. The cellular dysfunction of Hm receptor would induce asthma, Parkinson's disease, Alzheimer's disease, and even cancer[11–15]. Therefore, it is a relentless pursuit for chemists to develop artificial systems to mimic signal transduction processes for drug screening and biosensing[16,17].

Up to now, several artificial GPCRs that could transmit signalling as their natural counterparts have been constructed. For example, a helical foldamer with similar structural features to a class of membrane-active fungal antibiotics was ligated to a water compatible, metal-centred binding site and a conformationally responsive

[1]State Key Laboratory of Food Science and Resources, Jiangnan University, Wuxi 214122, China. [2]International Joint Laboratory on Food Safety, Jiangnan University, Wuxi 214122, China. [3]Institute of Analytical Food Safety, School of Food Science and Technology, Jiangnan University, Wuxi 214122, China. [4]Analysis and Testing Center, Jiangnan University, Wuxi 214122, China. [5]Key Laboratory of Synthetic and Biological Colloids, Ministry of Education, Jiangnan University, Wuxi 214122, China. e-mail: xpyan@jiangnan.edu.cn

fluorophore. In this way, a membrane-bound synthetic receptor that responds to the binding of a ligand by undergoing a conformational change over several nanometres (deep into the phospholipid bilayer) was devoloped[18]. Recently, an artificial GPCR containing three functional modules (a lipid-anchored cholic acid headgroup, a foldamer transmembrane moiety, and a precatalyst tailgroup) was developed to achieve controllable ON/OFF signal transduction through a conformational change between the folding and unfolding of a transmembrane foldamer moiety[19]. In spite of the importance of the wettability change of the hydrophobic layer for the activation of GPCRs in living organisms, no study on the design of artificial GPCRs based on the wettability change of the hydrophobic layer has been reported so far. Besides, current artificial GPCRs can only work in an environment mosaicked in fragile and unstable phospholipid bilayers, significantly hampering their application in vitro.

The solid-state nanopore strategy is very attractive in biomimetic nanoscience[20–25]. This strategy is powerful for the construction of artificial systems to simulate the signal transduction process in living organisms without the need for binding phospholipid bilayers[26–32]. In particular, the combination of polymer-based solid-state nanochannels with key recognition factors found in living organisms allows to construct a diverse array of artificial nanosystems to emulate the structure and function of living organisms[33–40]. For instance, a CO-regulated artificial nanosystem in a single nanochannel of polyethylene terephthalate (PET) membrane was developed by introducing a dynamic coordination system found in smooth muscle cells based on the interaction between ferroporphyrin and carboxyl acid in the channels[41]. Recently, bioinspired high-density elastomeric channels based on the self-assembly of polyisoprene-b-poly4-vinylpyridine in polyimide (PI) nanochannels were proposed for ultra-mechanosensitive specific chloride ion transport as biological mechanosensitive channels[42]. Nevertheless, few reports on artificial GPCR based on solid-state nanopores are available. The only successful example is artificial adenosine receptors (ARs) constructed by introducing an adenosine-responsive aptamer to the PET membrane, in which the conformation change can be regulated by adenosine, triggering a signal transmitting information[43]. Thus, the design of an artificial Hm receptor based on a polymer-based solid nanochannel to simulate the wettability-change-induced activation becomes a key issue.

Figure 1a illustrates the activation of natural GPCRs induced by wettability change. The hydrophobic cavity inside the receptor is transformed into a hydrophilic cavity when ligand-binding occurs. As a result, large number of water molecules are allowed to rush into the receptor, which finally changes the configuration of the receptor[44–46]. In addition, the ligand-binding pocket on the extracellular side of the natural receptors is widely acknowledged as the pivotal site for Hm recognition. The polar residues surrounding this region, especially those with phenolic hydroxyl and carboxylic groups (aspartic acid, asparagine, and threonine), play vital roles in the binding and recognition process of Hm[47].

Here, we report an artificial receptor model to simulate the activation of GPCR based on Hm-modulated wettability switching in a bionic nanochannel. Incorporation of key factors (polar residues and hydrophobic environment) into a polymer-based solid nanochannel to simulate Hm receptor activation represents a judicious choice. So, the inner surface of this bioinspired nanochannel is functioned with L-lysine modified fluorescein isothiocyanate (L-lysine-FITC) containing polar groups (Fig. 1b). A deprotonation of FITC is triggered by Hm, and the lactone ring of FITC is thus opened to form carboxyl anion (Supplementary Fig. 1)[48–50]. Furthermore, the multi-noncovalent interactions (hydrogen bonding and π-π interaction) between Hm and L-lysine-FITC, which presents in living organisms, are also involved in this artificial system. The wettability on the inner surface subsequently increases, altering the conductance of the nanochannel from a low to a high state. In this case, the artificial Hm receptor turns to its activated state from a nonactivated state. Therefore, a Hm receptor activation is successfully simulated. In addition, the artificial receptor shows high gating ratio, good selectivity, and reversibility. The developed artificial receptor is promising for the application in drug screening and biosensing.

Results

Fabrication of the artificial Hm receptor

The artificial Hm receptor was constructed in a single ion-track PET (12 μm thick) membrane. First, the conical nanochannel was manufactured by an ion-track etching technique[51]. The as-fabricated conical PET nanochannel showed a large opening (ca. 400 nm) on the base side (Supplementary Fig. 2) and a small opening (ca. 28 nm, calculated) on the tip side (Supplementary information). The ion-track etching generated carboxyl groups on the inner surface of the channels. L-lysine-FITC was then grafted on the inner surface of the conical channel via a two-step covalent modification process (Fig. 2a). L-lysine was first introduced through a typical condensation reaction between the surface carboxyl groups of the conical channel and the amino groups of L-lysine. Furthermore, fluorescent molecule FITC reacted

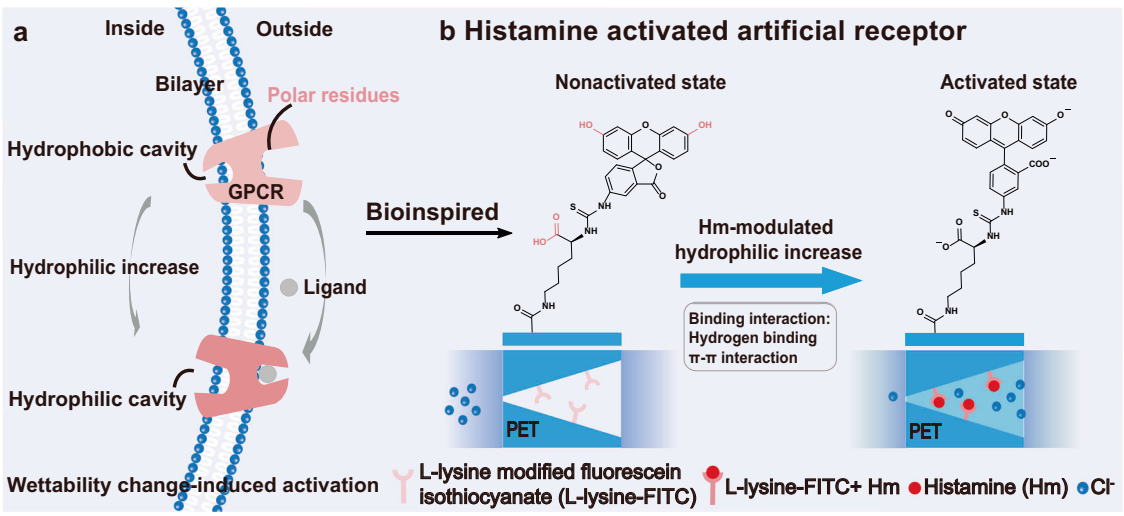

Fig. 1 | Scheme illustration of GPCRs. a Illustration of the transmembrane signalling process in natural GPCRs. **b** Illustration of the biomimetic Hm-modulated nanochannel and the Nonactivated/Activated switch of signal transduction process in a L-lysine-FITC modified artificial nanochannel.

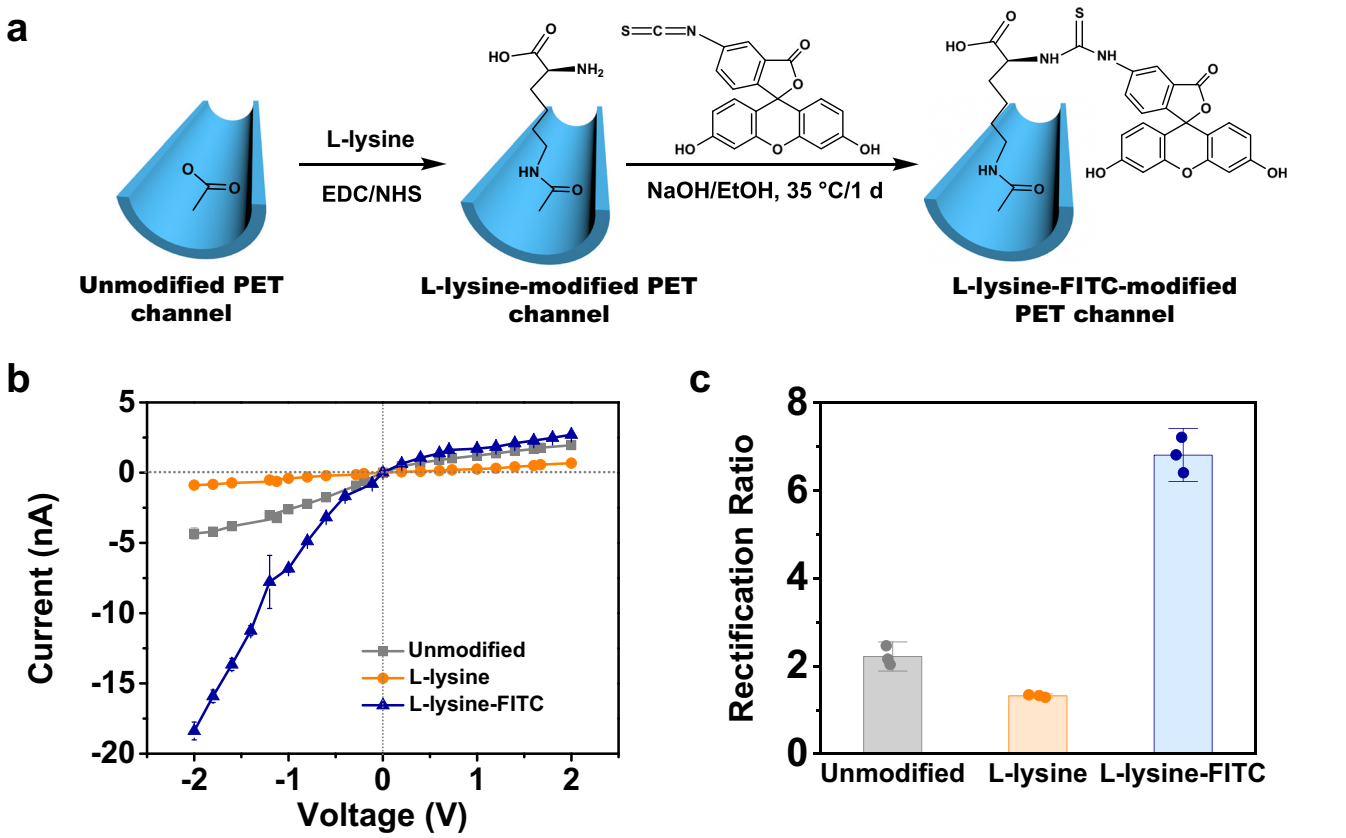

Fig. 2 | Fabrication of the artificial Hm receptor. a Fabrication processes. **b** Current-voltage (*I-V*) curves of the nanochannel before and after modification (0.1 M KCl, pH 7.0). **c** Rectification ratios of unmodified, L-lysine-modified, and L-lysine-FITC-modified nanochannel. Data are shown as mean ± SD ($n = 3$).

with amino groups on the L-lysine-modified nanochannel by nucleophilic addition reaction. The appearance of N *1 s* signal for L-lysine and a typical S *2p* signal for FITC in X-ray photoelectron spectra indicate the successful attachment of L-lysine and FITC on the inner surface of the PET conical nanochannel (Supplementary Figs. 3–5).

The successful modification of the conical PET nanochannel was further examined. The change in surface wettability of the PET film before and after modification was tested by contact angle measurements (Supplementary Fig. 6). The mean water contact angle of the membrane decreased from 63.6 ± 1.0° to 36.0 ± 1.6° after the introduction of L-lysine, and increased to 61.1 ± 0.7° after the decoration of L-lysine-FITC molecules due to the main hydrophobic nature of FITC. As shown in Fig. 2b, c, the unmodified channel exhibited ionic rectification behavior owing to the negative carboxyl groups as well as the asymmetric conical structure. Immobilization of L-lysine on the inner surface of the nanochannel obviously reduced the transmembrane ionic current and ionic rectification ratio because the amino group neutralized partial of the negative charges of the carboxyl groups (Supplementary Fig. 7), as confirmed by the zeta potential data (Supplementary Fig. 8). On the contrary, further introduction of FITC into the nanochannel led to significant increase in the current and ionic rectification ratio due to the increase in surface charge (Supplementary Figs. 7 and 8). These changes in ionic current also indicate the successful introduction of L-lysine and FITC to a PET nanochannel. All the above results prove the successful construction of the L-lysine-FITC-modified nanochannel.

Ionic rectification and gating performance of the artificial Hm receptor

Reversible closing and opening with the variation of pH creates a continuous structural change. This structural switching has been applied in biosensing[52]. However, in this work, the Hm-induced opening of the lactone ring in FITC molecule increases the surface wettability, which can be further strengthened after Hm capture on the inner surface of L-lysine-FITC-modified nanochannel through the hydrogen bonding and π-π interactions. Thus, an artificial model to mimic the wettability-induced activation of GPCRs is developed. The activation performance of the artificial receptor modulated by Hm was examined by current measurements. The ionic current and responsive ratio were used to characterize the activation of the artificial receptor. The responsive ratio (activated/nonactivated) is defined as $(I_{Hm} - I_0)/I_0$, where I_0 and I_{Hm} were the ionic current measured at −2 V before and after activation with Hm. The subsequent ionic current was measured in a 0.1 M KCl electrolyte solution at pH 5.0 because FITC underwent its intramolecular spirolactone form at pH 5.0. pH lower than 5.0 or higher than 5.0 would make FITC molecule lost the ability to own the intramolecular spirolactone form (Supplementary Figs. 9–16). After activation with 10 mM Hm, the ionic current at −2 V increased from −1.2 nA to −14.2 nA (Fig. 3a). Similarly, the responsive ratio at −2V increased from 0.1 to 11.3 (Fig. 3b). These changes in current and responsive ratio after activation by Hm arose from the surface wettability change of L-lysine-FITC-modified nanochannel. Although the increase of the hydrodynamic diameter of L-lysine-FITC upon binding with Hm (Supplementary Fig. 17) could enhance steric hindrance and reduce the ionic current, the ionic current still increased upon binding with Hm (Fig. 3a), indicating the surface charge and wettability played a dominant role in the ionic current[24]. The mean water contact angle of the L-lysine-FITC-modified film was 61.1 ± 0.7° before activation, but decreased to 50.7 ± 1.0° after the activation by Hm, indicating the increase in surface wettability (Fig. 3c). The Hm-induced conformational change of the FITC molecule and the hydrogen bonding and π-π interactions between Hm and the L-lysine-FITC molecule were also

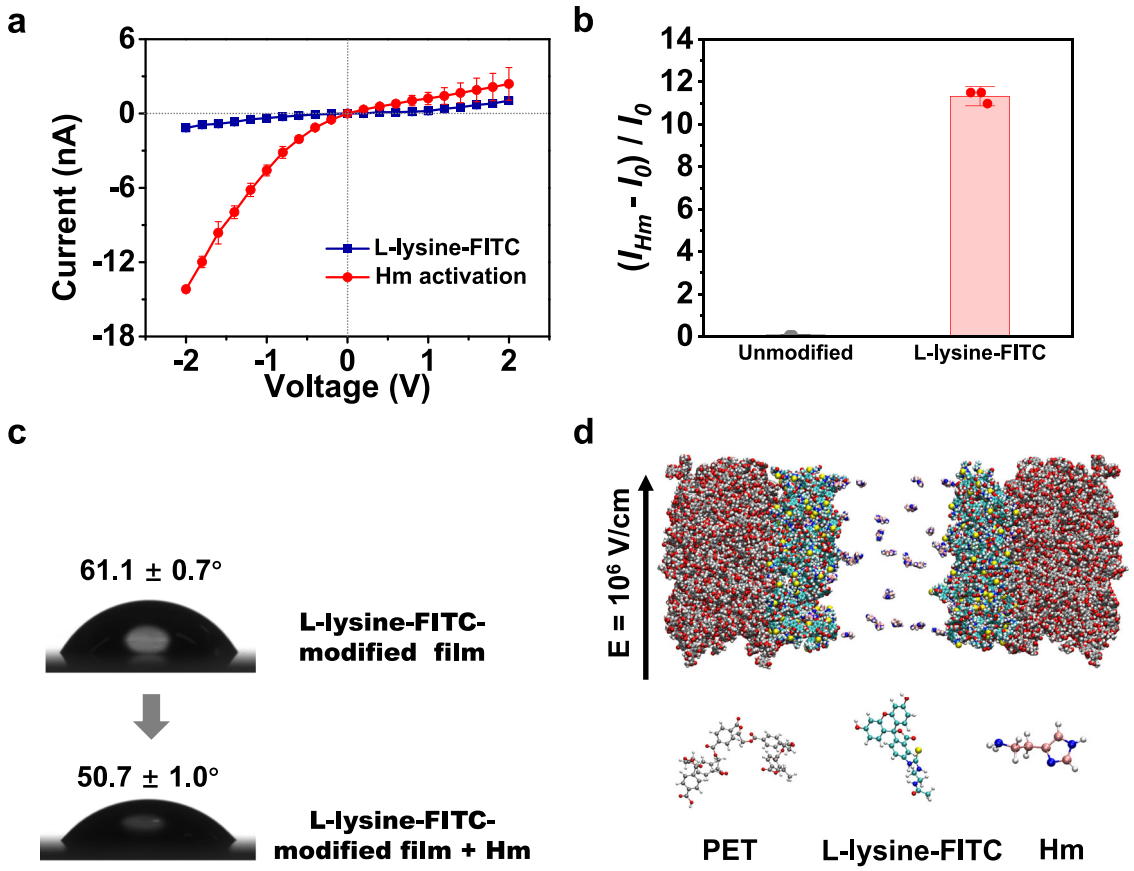

Fig. 3 | Response of the artificial receptor before and after activation by Hm. a *I-V* curves of L-lysine-FITC-modified nanochannel before and after Hm activation (0.1 M KCl, pH 5.0). **b** Responsive ratio of unmodified and L-lysine-FITC-modified nanochannel in the presence of Hm. **c** Change in the wettability of L-lysine-FITC-modified film. **d** Model diagram of Hm transport in L-lysine-FITC-modified nanochannel for MD simulation. Data are shown as mean ± SD ($n = 3$).

confirmed by ^{1}H NMR spectroscopy. The sequential addition of Hm into L-lysine-FITC in DMSO-d_6 resulted in the appearance of a new peak at 11 ppm and the disappearance of the peak at 10 ppm in ^{1}H NMR spectra, indicating the formation of carboxyl anion. Besides, remarkable downfield shifts and decay of both signals at 8.41, 8.25 and 7.84 ppm of phenyl protons (Supplementary Fig. 18a). The quantum chemistry calculation, density functional theory (DFT), further confirmed van der Waals force, hydrogen bonding, and π-π interactions between L-lysine-FITC and Hm (Supplementary Fig. 18b). In addition, the binding energy between L-lysine-FITC and Hm was calculated to be −76.94 kJ/mol.

We also conducted molecular dynamics (MD) simulation for further understanding the transport behavior of Hm through the artificial receptor. The simulation system of L-lysine-FITC nanochannel was represented with the system of PET, L-lysine-FITC, Hm and water (Fig. 3d). The change in hydrogen bond number, and mean square displacement (MSD) of Hm transport through L-lysine-FITC-modified nanochannel with time was then analyzed based on three replicates of simulations. The results show that the hydrogen bond number changed from 10 to 15 as the time increased to 100 ns, indicating that L-lysine-FITC could bind to Hm through hydrogen bonding (Supplementary Fig. 18c). The linear relationship between MSD and time demonstrates the effective diffusion of Hm within L-lysine-FITC-modified nanochannel (Supplementary Fig. 18d). UV-vis spectra further confirmed the molecular structure change of L-lysine-FITC (Supplementary Fig. 19). The above results show that Hm-modulated wettability switching on L-lysine-FITC-modified nanochannel was successfully achieved to mimic the activation of natural receptor.

Responsive rate, switchability, selectivity and specificity

The kinetic response of the artificial receptor L-lysine-FITC-modified nanochannel to Hm was then evaluated. As the ionic current increased slightly at 2 V with responsive time (Supplementary Fig. 20), the kinetic Hm response behavior was further charactered by analyzing the ionic current at −2 V. In the presence of 10 mM Hm, the ionic current and responsive ratio at −2 V remarkably increased with responsive time, reached the maximum −20.7 nA and 11.3 at 60 min, respectively (Fig. 4a, b). However, the ionic current and responsive ratio no longer changed with further increase of responsive time due to the reaction equilibrium between Hm and L-lysine-FITC.

The effect of Hm concentration on the activation of the artificial receptor L-lysine-FITC-modified nanochannel was further studied by *I-V* curves. The ionic current increased significantly at −2 V, but slightly at 2 V with Hm concentration (Fig. 4c and Supplementary Fig. 21a). The same is also true for responsive ratio (Fig. 4d and Supplementary Fig. 21b). The increase of ionic current and responsive ratio with Hm concentration resulted from the enhancement of the surface wettability in L-lysine-FITC-modified nanochannel due to continuous deprotonation reaction (Fig. 3c and Supplementary Fig. 1). Moreover, the ionic current and responsive ratio increased sensitively even at Hm concentration as low as 1 nM (Fig. 4c, d). When the Hm concentration increased to 10 mM, the ionic current reached −17.5 nA at −2 V, corresponding to a high responsive ratio of 11.3. These results show the Hm sensitive activation of the artificial receptor L-lysine-FITC-modified nanochannel.

The reversibility of the different states of the artificial receptor was demonstrated by measuring the ionic current at -2 V with alternate addition of Hm and HCl in the artificial receptor L-lysine-FITC-modified

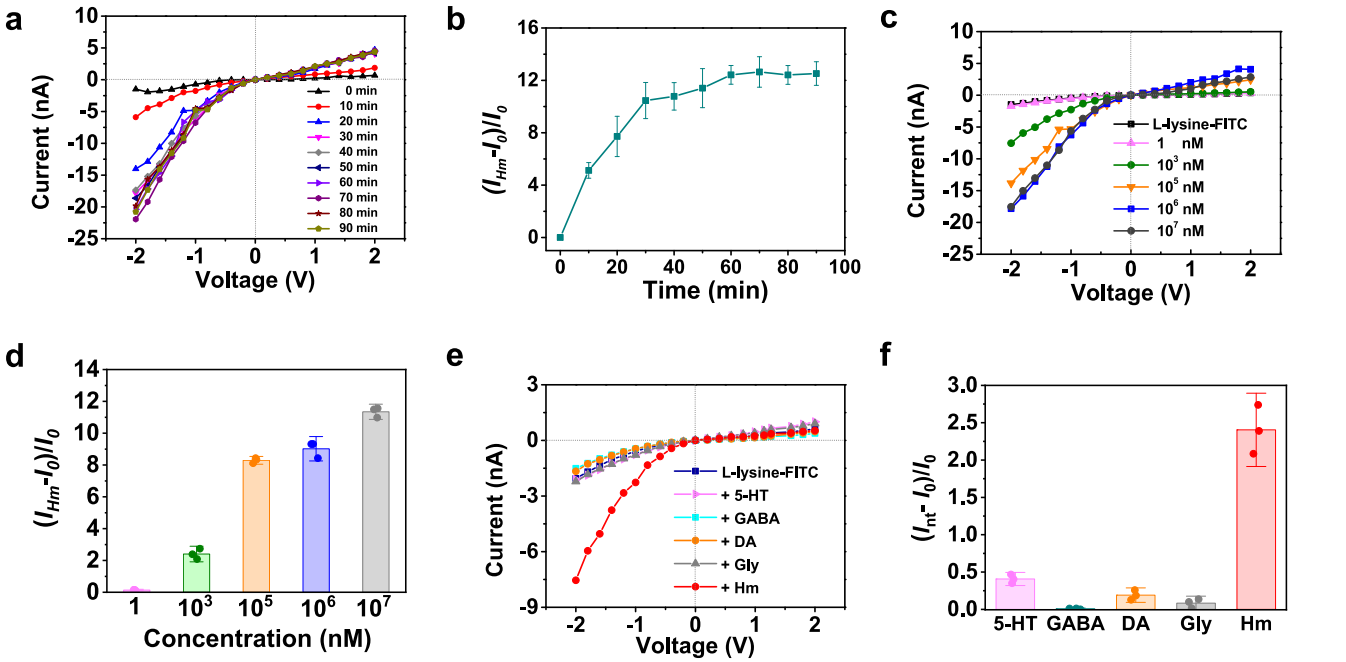

Fig. 4 | Performance of the artificial Hm receptor. Time-dependence of *I-V* curve (**a**), and responsive ratio at −2 V (**b**) for L-lysine-FITC-modified nanochannel after activation by 10 mM Hm. Hm concentration dependent *I-V* curves (**c**) and responsive ratio (**d**). *I-V* curves (**e**) and responsive ratio (**f**) of L-lysine-FITC-modified nanochannel after activation with 1.0 μM neurotransmitters. All current measurements were performed in 0.1 M KCl at pH 5.0. Data are shown as mean ± SD ($n = 3$).

nanochannel. The activated/nonactivated states of the smart artificial receptor could be switched upon the alternate addition of Hm and HCl (Supplementary Fig. 22a). No significant change in *I-V* curves after repeating this process several times indicates the excellent switchability and stable reversibility of this artificial receptor (Supplementary Fig. 22b).

The selectivity for the Hm-modulated activation of the developed artificial receptor was further investigated. To this end, other representative competitive neurotransmitters including 5-hydroxytryptamine(5-HT), γ-aminobutyric acid (GABA), dopamine (DA), glycine (Gly) were used as modulators and their corresponding *I-V* curves and responsive ratio were measured for comparison. The ionic current and responsive ratio at −2 V significantly increased after Hm-modulated activation of the artificial receptor, but only slightly changed in the presence of other neurotransmitters of 5-HT, GABA, DA, and Gly (Fig. 4e, f). These results indicate the excellent selectivity of the artificial nanochannel for Hm. This could be ascribed to the strong ability of Hm to grab protons from the phenolic hydroxyl group of FITC, which led to the opening of lactone rings in FITC efficiently. Our hypothesis was further supported by fluorescence measurement. Hm made a much greater enhancement of the fluorescence intensity of the L-lysine-FITC-modified nanochannel than other neurotransmitters (Supplementary Fig. 23).

Ethylenediamine (EDA) instead of L-lysine was used to further reveal the specificity of the artificial receptor (Supplementary Fig. 24). The variation in ionic current in the EDA-FITC-modified nanochannel was much smaller than in the L-lysine-FITC-modified nanochannel after the addition of Hm (Supplementary Fig. 25a). The responsive ratio of EDA-FITC and L-lysine-FITC modified nanochannels was 0.6 and 11.3, respectively (Supplementary Fig. 25b). As the carboxylic groups from the L-lysine in L-lysine-FITC molecule also have the ability to give protons to Hm, the surface charge of the L-lysine-FITC-modified nanochannel was enhanced in the presence of Hm. However, the EDA in EDA-FITC-modified nanochannel has no such protons to give to Hm, so no obvious change in the surface charge of EDA-FITC-modified nanochannel occurs upon adding Hm. To support this explanation, the compound EDA-FITC was prepared (Supplementary Figs. 26–29), and the zeta potentials of L-lysine-FITC and EDA-FITC were measured before and after adding Hm (Supplementary Fig. 30). Hm made the zeta potential of L-lysine-FITC change significantly (from −3.2 ± 0.4 to −18.0 ± 0.8 mV), but had that of EDA-FITC change slightly (from −3.3 ± 0.2 to −4.2 ± 0.3 mV). Moreover, the lactone ring of FITC in EDA-FITC-modified nanochannel more likely opens than in L-lysine-FITC-modified nanochannel at pH 5.0 (Supplementary Figs. 9 and 31). The mean contact angle of EDA-FITC-modified PET film are 68.7 ± 0.2° and 68.4 ± 0.1° with and without Hm, respectively (Supplementary Fig. 32). However, the mean contact angle of the L-lysine-FITC-modified film decreased from 61.1 ± 0.7° to 50.7 ± 1.0° by Hm (Fig. 3c). Therefore, Hm made a more significant change of the surface wettability and charge in L-lysine-FITC-modified nanochannel than in EDA-FITC-modified nanochannel. This observation verified the effective modulation of the artificial receptor L-lysine-FITC-modified nanochannel by Hm.

Potential for drug screening

We used the artificial receptor L-lysine-FITC-modified nanochannel to demonstrate its practical advantages for drug screening. For this purpose, we choose two typical antihistamines, levocetirizine dihydrochloride (LD) and loratadine (LA), to investigate their competitive inhibition of Hm-modulated activation of the developed artificial receptor. As shown in Fig. 5a, the ionic current increased from −2.5 nA to −4.3 nA after activation by 1 μM Hm. However, the ionic current significantly reduced when LD and LA were introduced to the artificial receptor system, indicating the excellent inhibition ability of these antihistamines. It is worth noting that LD inhibited Hm-modulated activation of the developed artificial receptor much more effectively than LA. The kinetic response of the Hm-activated artificial receptor to LA and LD have been investigated by analyzing the current at -2 V. In the presence of LD and LA, the current at -2 V decreased as responsive time increased to 5 min, then reached equilibrium (Fig. 5b, Supplementary Fig. 33a, Supplementary Fig. 34a). We have also evaluated the effect of LD and LA concentration on the inhibition ability to the Hm-activated artificial receptor. The ionic current of Hm-activated artificial receptor at −2 V decreased as the concentration of LD and LA increased, and LD always exhibited less current reduction than LA

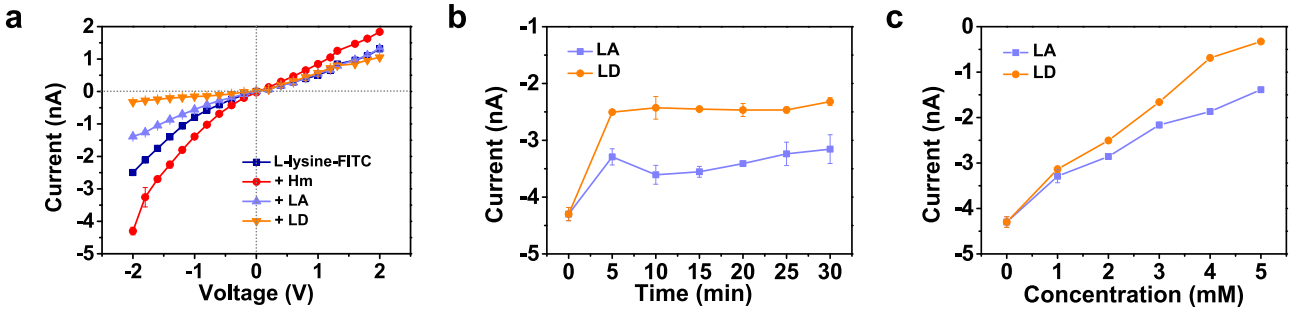

Fig. 5 | Potential drug screening application of the artificial Hm receptor. a *I-V* curves of L-lysine-FITC modified nanochannel with and without Hm, LD, and LA. **b** Time-dependence of current at −2 V of Hm-activated L-lysine-FITC modified nanochannel with LD, and LA. **c** Concentration-dependence of current at −2 V of Hm-activated L-lysine-FITC modified nanochannel with LD, and LA. Data are shown as mean ± SD ($n = 3$).

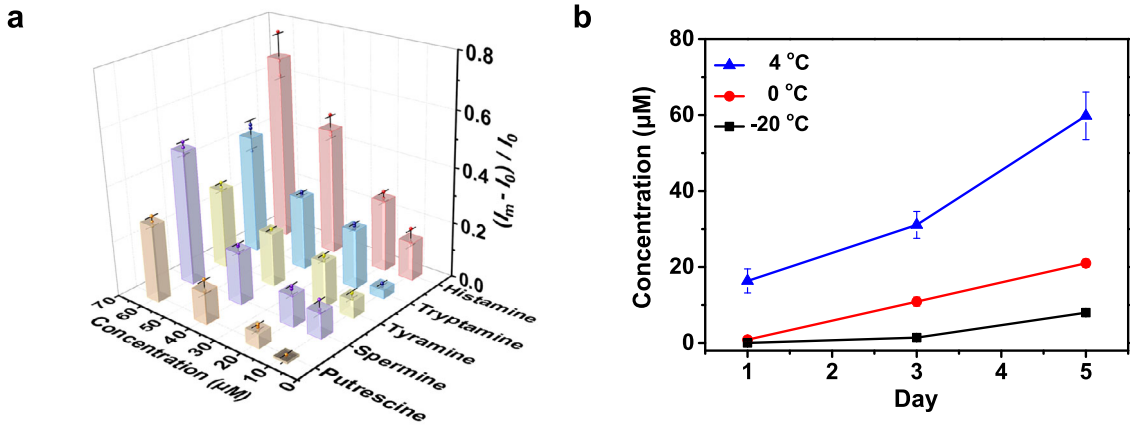

Fig. 6 | Application of the L-lysine-FITC-modified nanochannels as a biosensor. a Responsive ratio of L-lysine-FITC-modified nanochannels towards five biogenic amines with different concentrations. **b** Monitoring the freshness of shrimp at different temperatures within five days using the L-lysine-FITC-modified multiple nanochannels. Data are shown as mean ± SD ($n = 3$).

(Fig. 5c, Supplementary Fig. 33b, Supplementary Fig. 34b). These results reveal that the developed artificial receptor L-lysine-FITC-modified nanochannel is promising as an in vitro model for practical drug screening.

Potential for biosensing

We finally investigated the potential application of the artificial receptor L-lysine-FITC-modified nanochannel as an electrochemical sensor for biogenic amines. To this end, L-lysine-FITC-modified multiple nanochannels were prepared as the biosensor under the same conditions with the single nanochannel. The responsive behavior of the biosensor to Hm and other organic amines including spermine, tryptamine, putrescine, and tyramine was then examined since these organic amines are the important components of biogenic amines released by degradation of amino acids. The electrochemical sensor exhibited different responses to these amines. The change of responsive ratio with the concentration and type of the biogenic amine reveals the recognition capacity of the biosensor (Fig. 6a).

The practicability of the developed biosensor was evaluated by analyzing real samples. A good linear relationship ($R^2 = 0.9892$) between the concentration of Hm and responsive ratio in the range 1 − 60 μM were observed (Supplementary Fig. 35d). The developed biosensor gave a detection limit (3 s) of 0.02 μM Hm. For the analysis of real samples, Hm was detected in perch samples with the concentration of 7.97 ± 0.45 μM ($n = 3$). In addition, 20 μM Hm was spiked into shrimp and perch real samples, and the recoveries of Hm ranged from 85.7% to 102.7% (Supplementary Table 1), indicating no significant matrix interference. The developed biosensor was further explored to monitor the freshness of seafoods. It was found that the concentration of Hm in shrimp or the mixture sample (shrimp and perch) increased with storage time and temperature while higher storage temperature resulted in higher concentration of Hm (Fig. 6b and Supplementary Fig. 36). These results demonstrate that the feasibility of the developed biosensor for monitoring the freshness of seafood.

Discussion

In conclusion, we have developed an artificial receptor, L-lysine-FITC-modified nanochannel to mimic transmembrane signal transmission of biological GPCRs mechanism. The Hm-modulated wettability change in the L-lysine-FITC-modified nanochannel enables the switching of the conductance of the L-lysine-FITC-modified nanochannel from a low to a high state due to Hm induced opening of the lactone ring in FITC molecule, as well as multi-noncovalent interactions (hydrogen bonding and π-π interaction) between Hm and the L-lysine-FITC molecule. In this way, the artificial Hm receptor turns from a nonactivated state to a activated state in the presence of Hm. The stimulation of hydrochloric acid restores the lactone ring in FITC molecule to turn the artificial receptor to the nonactivated state. In this way, the activation/deactivation of the signal transduction in L-lysine-FITC-modified nanochannel can be regulated easily by Hm. The opening/closing of the lactone ring in FITC molecule enables mimicking the wettability-induced transduction of GPCRs mechanism in living organism. The developed Hm-modulated wettability switching in a bionic nanochannel has great potential applications in medicinal chemistry, biosensors, and healthcare systems.

Methods

Fabrication of the PET conical nanochannel

An ion track-etching technique was used to fabricate the conical nanochannel. The PET foil was irradiated with swift heavy ions having an energy of 11.4 MeV/Nucleon at the UNILAC linear accelerator (GSI, Darmstadt, Germany) with 10^7 ions·cm^{-2} ion tracks and single ion track. First, both sides of the ion-irradiated PET foil were exposed to UV light (365 nm) for 1 h in order to speed up the preparation of the conical channel. Before etching, the PET foil was embedded between two Teflon modules at 35 °C for 30 min (Supplementary Fig. 37). Then, the etching solution (9 M NaOH) was injected into one chamber of the Teflon modules, and the stopping solution (1 M KCl + 1 M HCOOH) was injected into the other chamber. The etching process was monitored by applying a potential of 1 V at both ends of the membrane by using Pt electrodes. The transmembrane current reflects the degree of etching. Therefore, the etching process was stopped by the stopping solution when the transmembrane current reached the desired current value. Finally, the PET foil was rinsed several times and immersed in deionized water to remove residual salts. In order to investigate the morphology and diameters of the base and tip sides of the single conical nanochannels, the multiple nanochannels with a pore density of 10^7 cm^{-2} were fabricated under the same etching conditions.

Nanochannel functionalization

The formation of carboxyl groups on the inner surface of unmodified multiple nanochannels during the etching process provides the opportunity to modify L-lysine on the channel surface via a typical coupling strategy. Specifically, the carboxyl groups would form an amine-reactive ester intermediate with N-hydroxysulfosuccinimide (NHS) in the presence of the cross-linker 1-ethyl-3-(3-dimethyllaminopropyl) carbodiimide (EDC). Then, the ester intermediate continued to react with the amino group in L-lysine to form an amide bond. Here, the well-etched PET foil was immersed into a 5 mL solution of 75 mg EDC and 15 mg NHS for 1.5 h at room temperature to form an ester intermediate. Following washing with deionized water three times, the PET foil was then transferred into the optimal reaction condition, 2 mM L-lysine or EDA solution overnight (Supplementary Figs. 38–42, Supplementary Tables 2–5). After washing the L-lysine-modified nanochannel or EDA-modified nanochannel with deionized water three times, the L-lysine-FITC-modified nanochannel was prepared by cross-linking the amine groups in L-lysine or EDA with isothiocyano groups of FITC molecules. Typically, L-lysine or EDA-modified PET foil was immersed into 1 mM FITC ethanol solution at 35 °C for 24 h, then the PET foil was rinsed with ethanol until the supernatant was non-fluorescent.

Ion current measurement

As illustrated in Supplementary Fig. 37, the ion current across the PET film was measured on a 2450 SourceMeter (Keithley, US). The PET membrane was mounted between two chambers of a homemade conductivity cell. Ag/AgCl electrodes were used to measure the transmembrane potential and the anode was placed on the large opening (base side) while the cathode was placed on the small opening (tip side). Both sides of the chamber were filled with 0.1 M KCl electrolyte. The scanning voltage varied from −2 V to +2 V in a 21 s period.

Analysis of real samples

Shrimp and perch were selected to test the practical application of the developed L-lysine-FITC-modified nanochannel. Thick slices were acquired and mixture from the pectoral fin, halfway and posterior to the vent after cleaning. Each sample of the mixture (0.5 g) were weighted accurately into a 50 mL centrifuge tube, and 25 mL of water were added to homogenize for 5 min. After centrifugation (1633 g for 10 min), the supernatant was filtered with a 0.22 μm filter membrane, and was stored at 4 °C for preservation.

The 20 μM histamine solution was added to the prepared actual fish samples to test the practical application of the developed L-lysine-FITC-modified nanochannel. The histamine concentrations in the fish samples can be acquired semiquantitatively with the established electrochemical method by comparation of the current.

We also investigated the effectiveness of this L-lysine-FITC-modified nanochannel for monitoring the seafood freshness. Shrimps or the mixture sample (shrimp and perch) without pretreatment, as an example, were placed at −20, 0, and 4 °C for 5 days. The current changes of the L-lysine-FITC-modified nanochannel after reaction with the pretreated shrimp samples at three different temperatures were observed for a period, respectively.

Data availability

All the data supporting the findings of this study are present in the paper and the supplementary information. All data can be obtained from the corresponding author on request. Source data are provided with this paper.

References

1. Lemmon, M. A. & Schlessinger, J. Cell signaling by receptor tyrosine kinases. *Cell* **141**, 1117–1134 (2010).
2. Venkatakrishnan, A. J. et al. Molecular signatures of G-protein-coupled receptors. *Nature* **494**, 185–194 (2013).
3. Ye, L. et al. Activation of the A 2A adenosine G-protein-coupled receptor by conformational selection. *Nature* **533**, 265–268 (2016).
4. Bokoch, M. P. et al. Ligand-specific regulation of the extracellular surface of a G-protein-coupled receptor. *Nature* **463**, 108–112 (2010).
5. Fried, S. D. E. et al. Hydration-mediated G-protein–coupled receptor activation. *PNAS* **119**, e2117349119 (2022).
6. Yuan, S. et al. Activation of G-protein-coupled receptors correlates with the formation of a continuous internal water pathway. *Nat. Commun.* **5**, 4733 (2014).
7. Thangam, E. B. et al. The role of histamine and histamine receptors in mast cell-mediated allergy and inflammation: The hunt for new therapeutic targets. *Front. Immunol.* **9**, 1873 (2018).
8. Schwartz, J.-C., Pollard, H. & Quach, T. T. Histamine as a neurotransmitter in mammalian brain: neurochemical evidence. *J. Neurochem.* **35**, 26–33 (1980).
9. Watkins, R. & Davidson, I. W. F. Action of histamine on phasic and tonic components of vascular smooth muscle contraction. *Experientia* **36**, 582–584 (1980).
10. Barocelli, E. & Ballabeni, V. Histamine in the control of gastric acid secretion: a topic review. *Pharmacol. Res.* **47**, 299–304 (2003).
11. Maintz, L. & Novak, N. Histamine and histamine intolerance. *Am. J. Clin. Nutr.* **85**, 1185–1196 (2007).
12. Nieto-Alamilla, G. et al. The histamine H_3 receptor: structure, pharmacology, and function. *Mol. Pharmacol.* **90**, 649–673 (2016).
13. Whalen, T. C. & Gittis, A. H. Histamine and deep brain stimulation: the pharmacology of regularizing a brain. *J Clin Investig.* **128**, 5201–5202 (2018).
14. Hu, W. & Chen, Z. The roles of histamine and its receptor ligands in central nervous system disorders: An update. *Pharm. Ther.* **175**, 116–132 (2017).
15. Massari, N. A., Nicoud, M. B. & Medina, V. A. Histamine receptors and cancer pharmacology: an update. *Br. J. Pharmacol.* **177**, 516–538 (2020).
16. Langton, M. J., Scriven, L. M., Williams, N. H. & Hunter, C. A. Triggered release from lipid bilayer vesicles by an artificial transmembrane signal transduction system. *J. Am. Chem. Soc.* **139**, 15768–15773 (2017).

17. Salahpour, A. et al. BRET biosensors to study GPCR biology, pharmacology, and signal transduction. *Front. Endocrinol.* **3**, 1–9 (2012).
18. Lister, F. G. A. et al. Ligand-modulated conformational switching in a fully synthetic membrane-bound receptor. *Nat. Chem.* **9**, 420–425 (2017).
19. Pang, S. et al. Folding and unfolding of a fully synthetic transmembrane receptor for ON/OFF signal transduction. *J. Am. Chem. Soc.* **145**, 20761–20766 (2023).
20. Pérez-Mitta, G. et al. Bioinspired integrated nanosystems based on solid-state nanopores: iontronic transduction of biological, chemical and physical stimuli. *Chem. Sci.* **8**, 890 (2017).
21. Zhang, Z., Wen, L. & Jiang, L. Bioinspired smart asymmetric nanochannel membranes. *Chem. Soc. Rev.* **47**, 322 (2018).
22. Fried, J. P. et al. In situ solid-state nanopore fabrication. *Chem. Soc. Rev.* **50**, 4974 (2021).
23. Guo, W., Tian, Y. & Jiang, L. Asymmetric ion transport through ion-channel-mimetic solid-state nanopores. *Acc. Chem. Res.* **46**, 2834–2846 (2013).
24. Hou, X., Zhang, H. & Jiang, L. Building bio-inspired artificial functional nanochannels: from symmetric to asymmetric modification. *Angew. Chem. Int. Ed.* **51**, 5296–5307 (2012).
25. Wei, R. et al. Stochastic sensing of proteins with receptor-modified solid-state nanopores. *Nat. Nanotechnol.* **7**, 257 (2012).
26. Xin, W. et al. Biomimetic KcsA channels with ultra-selective K^+ transport for monovalent ion sieving. *Nat. Commun.* **13**, 1701 (2022).
27. Zhao, C. et al. Bioinspired self-gating nanofluidic devices for autonomous and periodic ion transport and cargo release. *Adv. Funct. Mater.* **29**, 1806416 (2019).
28. Sun, Y. et al. A biomimetic chiral-driven ionic gate constructed by pillar [6] arene-based host-guest systems. *Nat. Commun.* **9**, 2617 (2018).
29. Xie, G. et al. Bacteriorhodopsin-inspired light-driven artificial molecule motors for transmembrane mass transportation. *Angew. Chem. Int. Ed.* **57**, 16708–16712 (2018).
30. Li, P. et al. Light-Driven ATP Transmembrane transport controlled by DNA nanomachines. *J. Am. Chem. Soc.* **140**, 16048–16052 (2018).
31. Xiao, K. et al. Biomimetic peptide-gated nanoporous membrane for on-demand molecule transport. *Angew. Chem. Int. Ed.* **57**, 151–155 (2018).
32. Sun, Z. et al. Fabrication of cysteine-responsive biomimetic single nanochannels by a thiolyne reaction strategy and their application for sensing in urine samples. *Adv. Mater.* **26**, 455–460 (2014).
33. Quan, J. et al. A visible-light-regulated chloride transport channel inspired by rhodopsin. *Angew. Chem. Int. Ed.* **60**, 2892–2897 (2021).
34. Yang, L. et al. Construction of a high-flux protein transport channel inspired by the nuclear pore complex. *Angew. Chem. Int. Ed.* **60**, 24443–24449 (2021).
35. Cheng, M. et al. A funnel-shaped chloride nanochannel inspired by ClC protein. *Nano Lett* **21**, 4086–4091 (2021).
36. Shang, X. et al. An artificial CO_2 -driven ionic gate inspired by olfactory sensory neurons in mosquitoes. *Adv. Mater.* **29**, 1603884 (2017).
37. Yang, L. et al. Chiral transport in nanochannel based artificial drug transporters. *Small* **19**, 2205274 (2023).
38. Li, M. et al. Functional nanochannels for sensing tyrosine phosphorylation. *J. Am. Chem. Soc.* **142**, 16324–16333 (2020).
39. Zhang, Y. et al. Chemically functionalized conical PET nanopore for protein detection at the single-molecule level. *Biosens. Bioelectron.* **165**, 112289 (2020).
40. Yang, L., Kong, X.-Y. & Wen, L. Bio-inspired nano-/micro-channels via supramolecular assembling: From fundamentals to applications. *Supramol. Mater.* **2**, 100043 (2023).
41. Xu, Y. et al. Smooth muscle cell-mimetic CO-regulated ion nanochannels. *Adv. Mater.* **28**, 10780–10785 (2016).
42. Li, C. et al. Ultra-mechanosensitive chloride ion transport through bioinspired high-density elastomeric nanochannels. *J. Am. Chem. Soc.* **145**, 19098–19106 (2023).
43. Li, P. et al. Adenosine-activated nanochannels inspired by G-protein-coupled receptors. *Small* **12**, 1854–1858 (2016).
44. Leioatts, N. et al. Retinal ligand mobility explains internal hydration and reconciles active rhodopsin structures. *Biochemistry* **53**, 376–385 (2014).
45. Chawla, U. et al. Activation of the G-protein-coupled receptor rhodopsin by water. *Angew. Chem.* **133**, 2318–2325 (1980).
46. Struts, A. V. et al. Osmotic stress studies of G-protein-coupled receptor rhodopsin activation. *Biophys. Chem.* **304**, 107112 (2024).
47. Xia, R. et al. Cryo-EM structure of the human histamine H_1 receptor/Gq complex. *Nat. Commun.* **12**, 2086 (2021).
48. Sjöback, R., Nygren, J. & Kubista, M. Absorption and fluorescence properties of fluorescein. *Spectrochim. Acta Part A* **51**, L7–L21 (1995).
49. McQueen, P. D., Sagoo, S., Yao, H. & Jockusch, R. A. On the intrinsic photophysics of fluorescein. *Angew. Chem. Int. Ed.* **49**, 9193–9196 (2010).
50. Jia, R. et al. Amine-responsive cellulose-based ratiometric fluorescent materials for real-time and visual detection of shrimp and crab freshness. *Nat. Commun.* **10**, 795 (2019).
51. Wang, J., Zhou, Y. & Jiang, L. Bio-inspired track-etched polymeric nanochannels: steady-state biosensors for detection of analytes. *ACS Nano* **15**, 18974–19013 (2021).
52. Martineau, M. et al. Semisynthetic fluorescent pH sensors for imaging exocytosis and endocytosis. *Nat. Commun.* **8**, 1412 (2017).

Acknowledgements

X.P.Y. is supported by the National Natural Science Foundation of China (No. 42421005 & 22176073). Z.Y.Y. is supported by the National Natural Science Foundation of China (No. 22206060).

Author contributions

Q.Z. acquired and analyzed data, developed the study concept and drafted the manuscript. X.Q.R. instructed the ion current experiment. Z.Y.Y. and H.L.Q. contributed to the improvement of the manuscript. X.P.Y. guided the project, proposed the study concept, interpreted the data and wrote the manuscript.

Competing interests

The authors declare no competing interest.

Additional information

Supplementary information The online version contains supplementary material available at https://doi.org/10.1038/s41467-025-57064-6.

Correspondence and requests for materials should be addressed to Xiu-Ping Yan.

Peer review information *Nature Communications* thanks the anonymous reviewer(s) for their contribution to the peer review of this work. A peer review file is available.